Towards a robust and efficient v^2-f implementation with application to transonic bump flow

By Georgi Kalitzin

1. Motivation and objectives

In the last few years, Durbin's v^2-f turbulence model has been extensively tested for subsonic and transonic flows using different numerics for the discretization of the equations and for their solution. Three versions of the model have been successively developed. The original model, Durbin (1995), includes a non-trivial wall boundary condition for the quantity f, which represents the pressure-strain term and is obtained from an elliptic relaxation equation. It also requires the distance to no-slip walls, albeit for the determination of the coefficient $C_{\epsilon 1}$ which regulates the production of dissipation of turbulent kinetic energy in the ϵ equation. The version developed by Parneix & Durbin (1997) defines a new expression for the coefficient $C_{\epsilon 1}$ substituting the distance to the wall with the ratio $\overline{v^2}/k$. Lien & Durbin (1996) developed another version of the model with a trivial wall boundary condition for f to improve the numerical robustness of the model, in particular for codes which solve equation by equation in a segregated manner.

An extensive, systematic comparison of each version has been conducted in Kalitzin (1999a) and Lien & Kalitzin (2000) for external flow around airfoils, wings, and over a bump. The conclusion of these studies was that all three versions predict in general very similar results for the potential flow region and most of the boundary layer. However, the $C_{\epsilon 1}(\overline{v^2}/k)$ definition causes an overprediction of the boundary layer growth rate in high Reynolds number flows with strong adverse pressure gradients. Forcing f to zero at no-slip walls has been found to delay transition. This is often desirable in transitional flow predictions, as RANS models generally trigger transition too far upstream. However, it has also been found responsible for a significant overprediction of skin friction in flow recovery regions, for example downstream of shock induced separation.

The present report is a continuation of this validation effort. It also describes the current implementation of Durbin's v^2-f turbulence model in the turbomachinery code TFLO, CITS (2000). This RANS code will be used in the framework of the Accelerated Strategic Computing Initiative (ASCI) at the Center for Integrated Turbulence Simulations (CITS) for large scale computations of flow through the compressor and turbine of an aircraft engine. This requires a robust and efficient implementation of the model. A three-factored scheme which is able to handle the wall boundary conditions of the original model has been developed for this purpose, and its description is included in the report.

2. v^2-f turbulence model

The v^2-f turbulence model is an advanced eddy-viscosity model. It can be regarded as an abbreviated Reynolds stress model consisting of three transport equations: for the

turbulent kinetic energy k, the dissipation of the turbulent kinetic energy ϵ, and for the scalar quantity $\overline{v^2}$. Close to solid walls the latter represents the energy of the fluctuations normal to the wall. The production term in the $\overline{v^2}$ transport equation is a pressure strain term. Its nonlocal dependency on the flow, in particular in the presence of solid walls, is modeled with an elliptic relaxation equation for a quantity f. The equations of the original model and of the modified version considered in the present study can be found in Durbin (1995) and Lien & Durbin (1996), respectively. These model versions will be referred to in this report as version A and B, respectively. The main differences between version A and B are the wall boundary conditions for f, which are: $f_w = -20\nu^2\overline{v_1^2}/\epsilon_w y_1^4$ and $f_w = 0$, respectively. Index w and 1 denotes the value at the wall and in the first cell above the wall, respectively. To enforce, in version B, the trivial condition for f at the wall, the term $5\epsilon\frac{\overline{v^2}}{k}$ has been subtracted from the $\overline{v^2}$ transport equation and added to the f equation. This modification preserves the correct asymptotic behavior of the quantity $\overline{v^2}$. The coefficients of version A and B are slightly different, most notable is the coefficient $C_{\epsilon 1}$, which regulates the production of dissipation of turbulent kinetic energy. In version A the coefficient $C_{\epsilon 1}$ is a function of the distance to the wall, and in version B it is a function of the ratio of $\overline{v^2}/k$.

3. Implementation of v^2-f in TFLO

The v^2-f model is solved in TFLO in a separate set of subroutines segregated from the mean flow. Multigrid is used for the mean flow, and at each multigrid cycle on the finest grid the model's subroutines are called. They return an updated value for the eddy viscosity and the turbulent kinetic energy. Only these two quantities are passed to the mean flow solver for the determination of the Reynolds stresses.

Different solution algorithms have been employed for each model version. In both versions, the k and ϵ equations are solved first in an implicit, pairwise coupled manner with a cell centered finite difference scheme. The f and $\overline{v^2}$ equations of version A are solved similarly coupled, allowing an implicit treatment of the f-wall boundary condition. The solution follows the description in Kalitzin (1999). The f equation in version B is solved separately with an elliptic solver. Its solution subsequently enters the production term in the $\overline{v^2}$ equation. The zero wall boundary condition for f basically decouples the f from the $\overline{v^2}$ equation. The net source term in the f equation is invariably non-negative, ensuring a non-negative solution f in the entire computational domain.

In both versions, the diffusion terms are discretized with second order central differences. First order upwind differences are used for the discretization of the convective terms. At the current stage, the model is implemented to provide a steady state solution by marching in time from an initial guess. The time derivative term is discretized with a first order forward difference. Local timesteps are used to accelerate convergence. These timesteps are determined by the spectral radius analysis from mean flow quantities, the eddy viscosity and the input CFL number. Multigrid is not used for the turbulence equations. The timesteps for the advancement of the turbulence variables have been weighted with a constant factor. Except for the f-equation in version B, the algebraic system of equations resulting from the implicit operators are solved with a three-factored, approximate factorization scheme. The f-equation in version B is solved with a conjugate gradient method.

Next, a factorization scheme is described which has been developed to handle the wall boundary conditions in the v^2-f model, version A. The f wall boundary condition is a

critical issue in the implementation. The value of f_w at the wall depends strongly on the value of $\overline{v^2}$ in the first cell above the wall (see also the profiles of the scalars $\overline{v^2}$ and f in Fig. 1 for flow over a flat plate). A small change of $\overline{v_1^2}$ in the first cell above the wall changes the value f_w at the wall, which affects in an elliptic manner the f distribution across the entire boundary layer. This requires an accurate solution of the model's equations close to solid walls.

The $\overline{v^2}$-f equations can be written in matrix form notation as:

$$(I + S + L_\eta + L_\xi + L_\zeta)\Delta\phi = RHS \tag{3.1}$$

whereby L_γ, with $\gamma = \xi, \eta, \zeta$, contains the convection and diffusion terms in a grid oriented (ξ, η, ζ) coordinate system. S and $\Delta\phi$ contain the implicitly treated source terms and the solution update, respectively. I is the identity matrix. RHS is the right-hand side.

A computer memory and CPU time efficient algorithm for the solution of Eq. (3.1) is critical in large three-dimensional computations. Ordinary ADI algorithms developed for structured grids often converge better if certain directions of the computational coordinate system are normal to walls. Only one direction may be normal to a solid wall for turbulence models with stiff wall boundary conditions as in the case of the v^2-f model. Even in a multi-block concept, this directionality of the factorization algorithm may lead to severe constrains for the grid generation process for complex geometries, especially in wall corners of cavities or wing-body junctions of an aircraft.

An ADI algorithm requires an approximation for Eq. (3.1), which allows a split into a set of one-dimensional equations. As proposed in Kalitzin *et al.* (2000) the approximation of Eq. (3.1) with

$$(I + S + L_\eta)\,(I + S)^{-1}\,(I + S + L_\xi)\,(I + S)^{-1}\,(I + S + L_\zeta)\,\Delta\phi = RHS \tag{3.2}$$

allows a split into the three one-dimensional equations

$$(I + S + L_\eta)\,\Delta\phi' = P \tag{3.3}$$

along η grid lines,

$$(I + S + L_\xi)\,\Delta\phi'' = (I + S)\Delta\phi' \tag{3.4}$$

along ξ grid lines, and

$$(I + S + L_\zeta)\,\Delta\phi''' = (I + S)\Delta\phi'' \tag{3.5}$$

along ζ grid lines. In contrast to earlier formulations in Krist (1998), the source terms are treated implicitly in each computational direction. This leads to a consistent implicit operator on the left-hand side in each computational direction and allows in the case of the v^2-f model different computational directions to be normal to solid walls.

The scheme described follows Klopfer *et al.* (1998). However, they derive a diagonally dominant scheme for the solution of the Navier-Stokes equations which does not include source terms. The efficiency of the scheme described is of the same order as of an ordinary factorization scheme.

4. Flow over flat plate

The current implementation of the v^2-f model in TFLO has been tested for subsonic flow over a flat plate. The flow is computed for a Reynolds number of $6 \cdot 10^6$ and a Mach

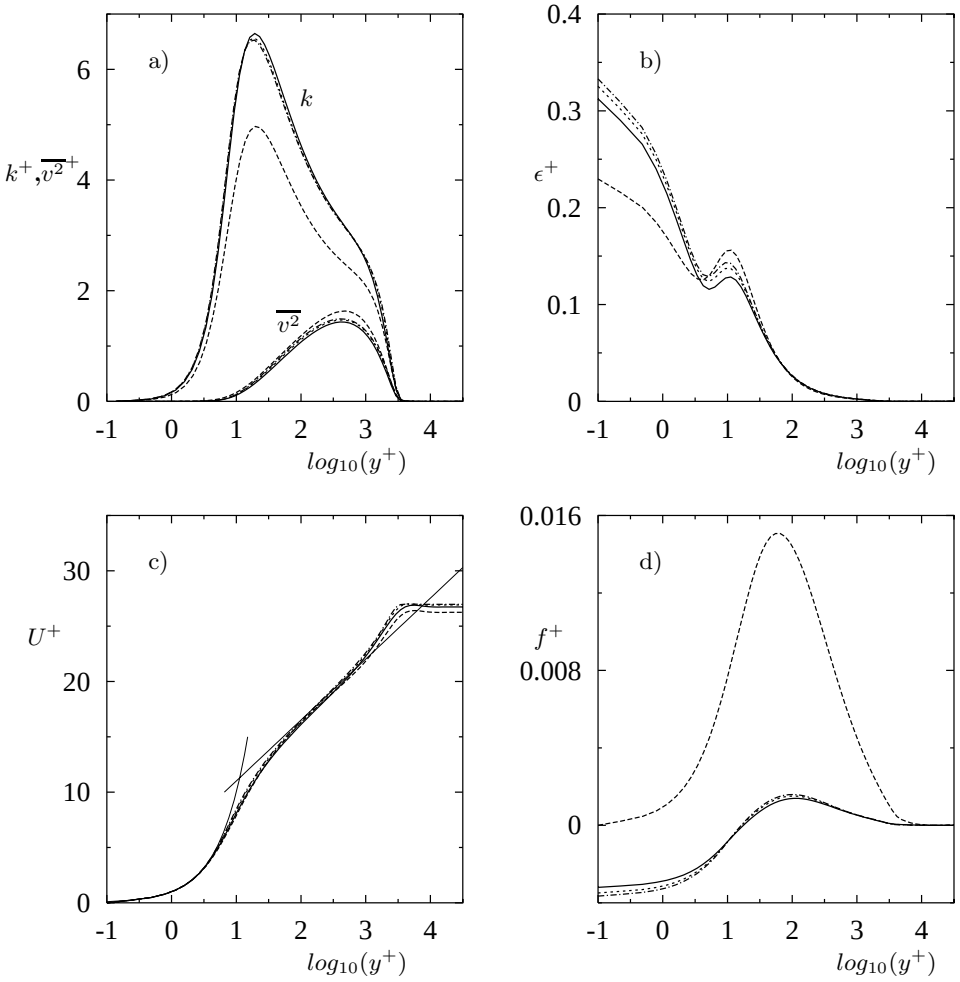

FIGURE 1. Profiles of a) k and $\overline{v^2}$ b) ϵ, c) U^+ and d) f for flow over a flat plate; v^2-f: — - — : version A, CFL3D; ····· : version A, TFLO, VIS4=0.3; ——— : version A, TFLO, VIS4=1.0 - - - - : version B, TFLO, VIS4=1.0).

number of 0.2. The mesh of 64×96 cells is provided with version 5 of CFL3D (Krist (1998)). An average of 40 grid points lie within the boundary layer.

A comparison of v^2-f results is shown in Fig. 1. The log law and profiles of the normalized turbulent quantities are shown for $x/c = 0.9$. The discrepancy in the results obtained with version A in TFLO and CFL3D (the latter code has been previously extensively validated against several applications) is particularly large for the ϵ and f distribution. It could be traced back to the numerical dissipation of the mean flow solver. While the turbulence transport equations are solved with a first order upwind scheme in both codes, the mean flow is solved in TFLO with a dissipation scheme of Jameson, Schmidt & Turkel (1981) and in CFL3D with an upwind flux difference splitting of Roe (1986). The discrepancy reduces by setting VIS4 in TFLO from the default value of 1 to 0.3, reducing the artificial fourth order background dissipation.

The same plots include the solution of version B. As shown in Fig. 1d, f is larger zero over the entire boundary layer, and its maximum value is significant larger than for version A. At the wall f is zero. As shown in Fig. 1a, $\overline{v^2}$ has the same asymptotic behavior approaching the wall as for version A. The peak value of the turbulent kinetic energy, k^+, is about 5, and this is significantly lower than for version A. While it corresponds to predictions with other models, this value might be too low. Turbulent kinetic energy profiles obtained with version A for the Bachalo-Johnson bump described next agree significantly better with the experiments.

The solution converged for both versions to a five orders of magnitude in the L_2 norm of the density, turbulent kinetic energy, and $\overline{v^2}$ residual in about 2000 iterations. This is usually required for this type of computation and comparable to other turbulence models. Version B converges more robustly and for a wider range of various numerical parameters.

5. Flow over Bachalo-Johnson bump

Transonic flow over the Bachalo-Johnson bump (Bachalo (1986)) has been chosen to study the performance of TFLO/v^2-f in predicting shock-boundary layer interaction. This test case is an axisymmetric configuration, and the flow is not dependent on the circumferential direction and is thus two-dimensional even in the case with massive separation. The flow is computed for an inflow Mach number of 0.873 and a Reynolds number of $Re_c = 2.66 \cdot 10^6$. The computational mesh consists of $192 \times 100 \times 8$ cells. The two-dimensional mesh, shown in Fig. 3, is the same as used in Kalitzin (1999) with some additional cells at the exit in order to split the mesh in several multigridable blocks. Cells are clustered in the region of the shock. The flow is computed fully turbulent, neglecting the influence of wind tunnel walls.

The pressure and skin friction distribution on the wall of the cylinder and bump are shown in Fig. 5. The bump geometry is shown in the background with the symmetry axis coinciding with the frame line. The x-coordinate is chosen such that the bump is located between 0 and 1. Note that the C_p-axis in the pressure plot is reversed. Versions A and B predict roughly the same pressure distribution with the correct shock location and a slightly higher pressure in the separation region. The latter indicates that the separation bubble is underpredicted. The separation region is clearly visible in the negative skin friction in Fig. 5b. There is no experimental data for skin friction available. However, the plot shows that the flow computed with version B recovers faster with a significantly larger skin friction downstream of the separation region. This is consistent with the results obtained for the RAE 2822 airfoil in Lien & Kalitzin (2000).

In Figs. 2 and 4 velocity, shear stress, and turbulent kinetic energy profiles are shown for 6 stations, the location of which is indicated in Fig. 3. The Reynolds shear stress is consistently underpredicted for both versions, in particular in the separation region. Note that, as described in Johnson (1987), the comparison of shear stresses in a shear layer aligned coordinate system will result in better agreement of the computational and experimental data. The computed turbulent kinetic energy profiles differ significantly for both versions. As for the flat plate, Fig. 1a, the turbulent kinetic energy profiles obtained with version A are significantly larger and agree well with the experimental data.

Results for the same test case using the v^2-f model, version Parneix & Durbin (1997), the Spalart-Almaras, and Menter SST are given in Kalitzin (1999).

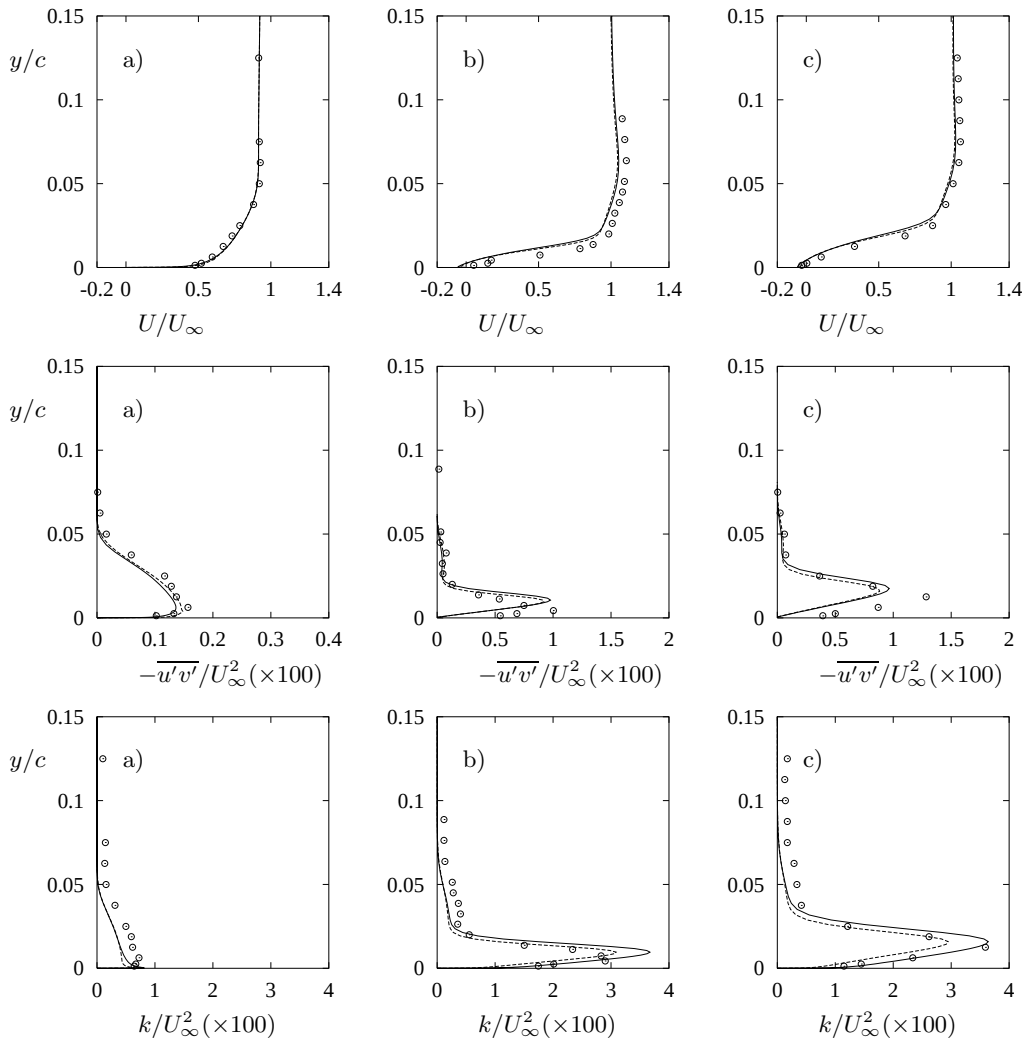

FIGURE 2. Bachalo-Johnson bump: velocity, shear-stress and turbulent kinetic energy; v^2-f: ——— : version A, – – – – : version B, ∘ : expt.

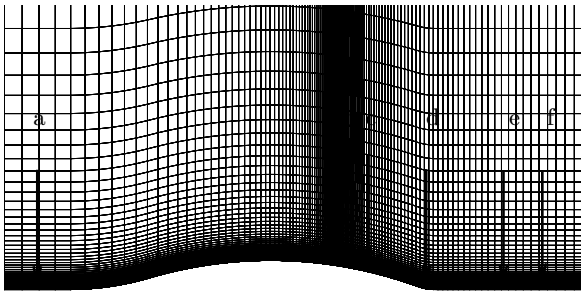

FIGURE 3. Bachalo-Johnson bump: computational mesh. x/c = -0.250 (a), 0.750 (b), 0.813 (c), 1.000 (d), 1.250 (e), 1.375 (f).

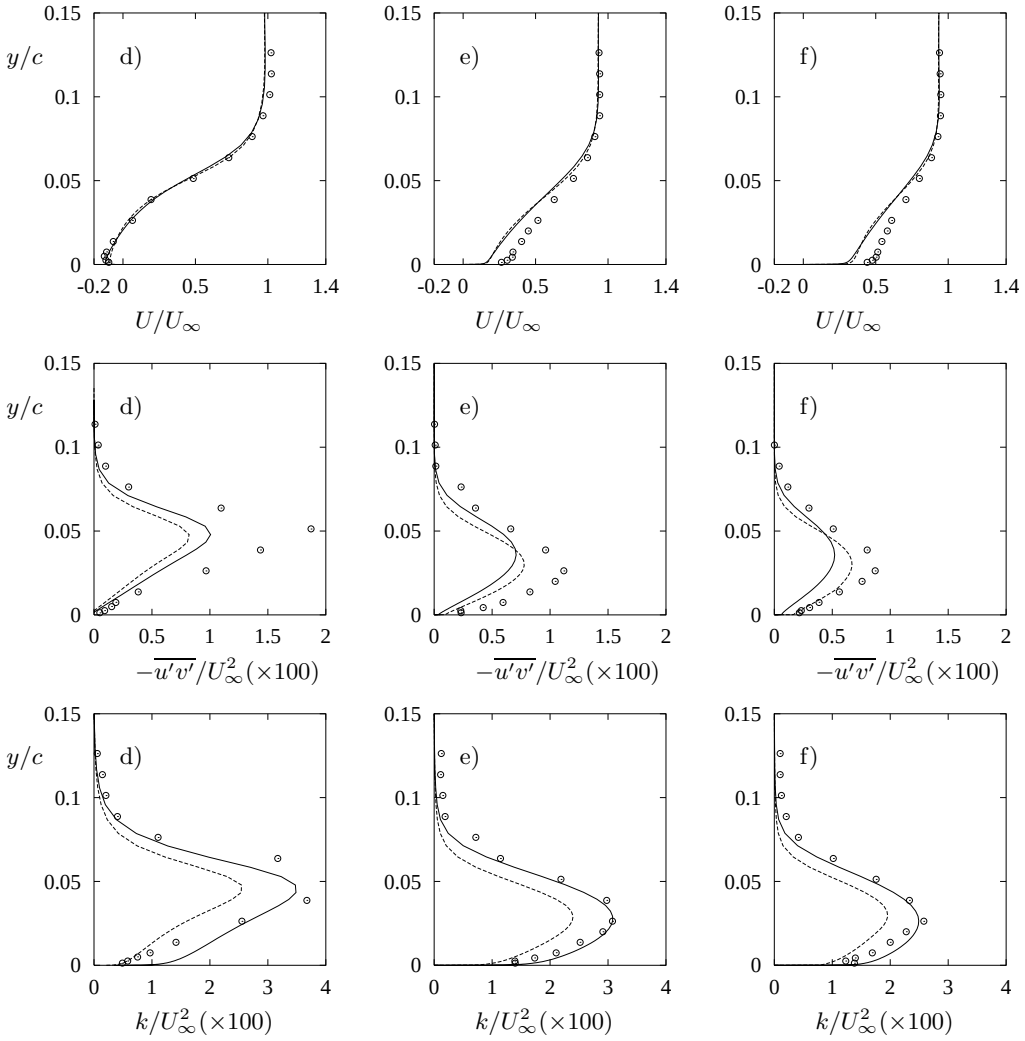

FIGURE 4. Bachalo-Johnson bump: velocity, shear-stress, and turbulent kinetic energy; (continuation); v^2-f: ——— : version A, – – – – : version B, ∘ : expt.

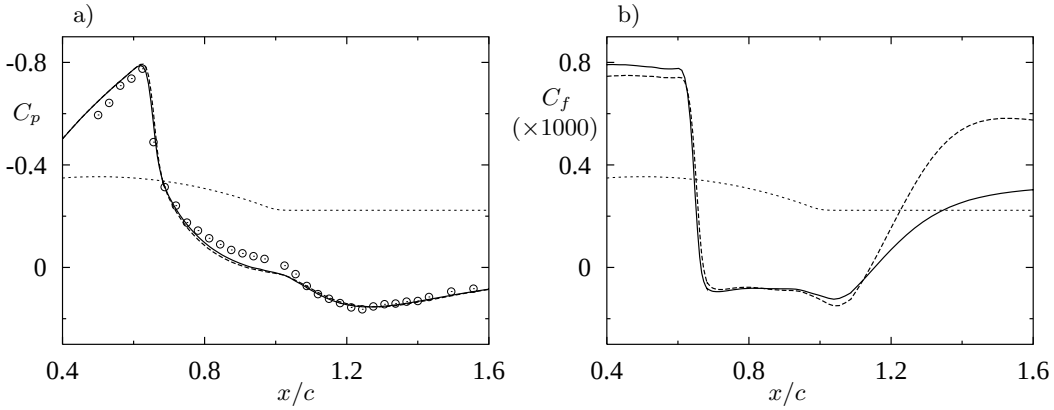

FIGURE 5. Bachalo-Johnson bump: a) pressure and b) skin friction dist.; v^2-f: ——— : version A, – – – – : version B, ∘ : expt.

6. Conclusions and future work

Two versions of the v^2-f model, version A and B, have been implemented in TFLO and successfully tested for 2 two-dimensional test cases. In both cases, subsonic flow over a flat plate and transonic flow over a axisymmetric bump, the TFLO/v^2-f code performs similarly in terms of accuracy and computational costs to previous v^2-f implementations.

The results for the Bachalo - Johnson bump support the conclusions from previous computations. Version A and B predict main differences in skin friction and turbulent kinetic energy profiles. The understanding of the cause of these differences is important for further development of the v^2-f model.

Version B is due to the zero f wall boundary condition being significantly more robust. In addition to the test cases presented, its implementation in TFLO has also been successfully tested for three-dimensional transonic flow at a turbine blade-endwall. The results for this test case will be described in a future report. Version B is currently being implemented in TFLO as the default version, and it is used for the initial iterations with the v^2-f model.

A three-factored approximate factorization scheme has been developed to handle the wall boundary conditions of version A. In contrast to earlier schemes, it allows any computational direction to be normal to solid walls. It is currently being tested for the turbine blade-endwall test case.

Future work includes the implementation in TFLO/v^2-f of a higher order time integration scheme which is required for unsteady computations. It is planned to implement a dual time stepping scheme in which a pseudo timestep is used for the inner iteration to a pseudo steady state. For rotational flows, modifications to the Boussinesq approximation proposed by Pettersson-Reif *et al.* (1999) will be investigated. These modifications were designed to sensitize the v^2-f model to mimic rotational effects on turbulence.

REFERENCES

Bachalo, W. D. & Johnson, D. A. 1986 Transonic turbulent boundary layer separation generated on an axisymmetric flow model. *AIAA J.* **24**, 437-443.

CITS 2000 *CITS - Center for Integrated Turbulence Simulations - Annual Technical Report.*

Durbin, P. A. 1995 Separated flow computations with the k-ε-v^2 model. *AIAA J.* **33**, 659-664.

Jameson, A., Schmidt, W. & Turkel, E. 1981 Solutions of the Euler Equations by Finite Volume Methods Using Runge-Kutta Time-Stepping Schemes. *AIAA 8l-1259.*

Johnson, D. A. 1987 Transonic separated flow predictions with an eddy-viscosity/Reynolds-stress closure model. *AIAA J.* **25**, 252-259.

Kalitzin, G. 1999a Application of the v^2-f model to aerospace configurations. *Annual Research Briefs,* Center for Turbulence Research, NASA Ames/Stanford Univ. 289-300.

Kalitzin, G., Kalitzin, N., & Wilde, A. 2000 A Factorization Scheme for RANS Turbulence Models and SNGR Predictions of Trailing Edge Noise. *AIAA 2000-1982.*

Kalitzin, G. 1999 Application of v^2-f turbulence model to transonic flows. *AIAA 99-3780.*

Klopfer, G. H., Hung, C. M., Van der Wijngaart, R. F. & Onufer, J. T. 1998

A Diagonalized Diagonal Dominant Alternating Direction Implicit (D3ADI) Scheme and subiteration correction. *AIAA 98-2824.*

Krist, S., Biedron, R. & Rumsey, C. 1998 CFL3D User's Manual (Version 5.0). *NASA/TM-208444.*

Lien, F. S. & Durbin, P. A. 1996 Non-linear $k - \varepsilon - \overline{v^2}$ modeling with application to high lift. *Proc. of the Summer Program*, Center for Turbulence Research, NASA Ames/Stanford Univ. 5-22.

Lien, F. S. & Kalitzin, G. 2000 Computations of transonic flow with the v^2-f turbulence model. *Int. J. of Heat and Fluid Flow.* **6238**, 1-9.

Parneix, S. & Durbin, P. A. 1997 Numerical simulation of 3D turbulent boundary layers using the V2F model. *Annual Research Briefs*, Center for Turbulence Research, NASA Ames/Stanford Univ. 135-148.

Pettersson-Reif. B. A., Durbin, P. A. & Ooi, A. 1999 Modeling rotation effects in eddy-viscosity closures. *Int. J. of Heat and Fluid Flow.* **20**, 563-573.

Roe, P. L. 1986 Characteristic Based Schemes for the Euler Equations *A Numerical Review of Fluid Mech.* 337-365.